Journal of Magnetism and Magnetic Materials 385 (2015) 243–249

Contents lists available at ScienceDirect

Journal of Magnetism and Magnetic Materials

journal homepage: www.elsevier.com/locate/jmmm

Crystal and magnetic structures, phase transitions in quasi-one-dimensional pyroxenes $Na_{0.5}Li_{0.5}FeGe_2O_6$

T.V. Drokina [a], G.A. Petrakovskii [a], M.S. Molokeev [a,b,*], S.V. Misyul [c], V.S. Bondarev [a,c], D.A. Velikanov [a,c], M. Frontzek [d], J. Schefer [d]

[a] L.V. Kirensky Institute of Physics, Siberian Branch of Russian Academy of Science, Akademgorodok, 50/38, Krasnoyarsk 660036, Russia
[b] Far Eastern State Transport University, str. Serysheva 47, Khabarovsk 680021, Russia
[c] Siberian Federal University, pr. Svobodny 59, Krasnoyarsk 660074, Russia
[d] Laboratory for Neutron Scattering and Imaging, Paul Scherrer Institut, CH-5232 Villigen PSI, Switzerland

ARTICLE INFO

Article history:
Received 10 February 2015
Accepted 5 March 2015
Available online 6 March 2015

Keywords:
Phase transition
Magnetic structure
Pyroxene
Magnetic properties
Calorimetric measurements

ABSTRACT

The possibility of cation substitution in pyroxenes allows the investigation the gradual change of structural and magnetic properties under doping in these compounds. Here, $Na_{0.5}Li_{0.5}FeGe_2O_6$ was prepared by the standard solid-phase reaction method and has been investigated using X-ray and neutron powder diffraction, and further characterized by magnetic and calorimetric measurements. The crystal structure of $Na_{0.5}Li_{0.5}FeGe_2O_6$ at 300 K is monoclinic $C2/c$ ($a=10.0333(1)$, $b=8.8136(1)$, $c=5.5295(9)$ Å, $\beta=108.921(1)^\circ$). Calorimetric investigations indicate a displacive first order phase transition at $T=271\pm1$ K which is accompanied by the appearance of superstructure reflections in the X-ray patterns. At this transition $Na_{0.5}Li_{0.5}FeGe_2O_6$ undergoes a space group change from $C2/c$ to $P2_1/c$ ($a=9.9692(3)$, $b=8.8545(3)$, $c=5.4752(2)$ Å, $\beta=108.494(1)^\circ$). Magnetic order has been found below the Néel temperature $T_N\approx18$ K and has been refined from neutron diffraction. The quasi-low-dimensional magnetic spin system $Na_{0.5}Li_{0.5}FeGe_2O_6$ exhibits a collinear antiferromagnetic structure with the space group P_a2_1/c and the doubling of the unit cell along the crystallographic a-axis of the pyroxene crystal (propagation vector $\boldsymbol{k}=(1/2, 0, 0)$). The critical modes which are responsible for the phase transition from $C2/c$ to $P2_1/c$ symmetry and for the magnetic transition from paramagnetic to antiferromagnetic state have been determined and their role in the transition is described. They are also the relevant mechanism driving the magnetic order in $LiFeGe_2O_6$.

1. Introduction

The pyroxenes compounds have the general chemical formula ABX_2O_6 (A=Na, Li and Ca; B=Mg, Cr, Cu, Ni, Fe, etc.; X=Ge, Si). They cover a broad class of a materials and have shown a variety of different magnetically ordered states (antiferromagnetic [1–4], ferromagnetic [3,5], modulated magnetic structure [6,7], spin gap state [8]). The variety of magnetic properties is connected to the features of the crystal structure which allows the existence of competing magnetic exchange interactions. Some pyroxene compounds have attracted significant theoretical interest due to their one-dimensional magnetism [9] and the structural phase transitions as a function of temperature and pressure [10–13]. Further, special interest to these systems comes from the properties of some pyroxene compounds ($NaFeGe_2O_6$, $NaFeSi_2O_6$, $LiFeSi_2O_6$ and $LiCrSi_2O_6$) which exhibit a strong interaction between the magnetic and electric order [14,15].

The crystal structure and magnetic properties of the compounds $NaFeGe_2O_6$, $LiFeGe_2O_6$ have been studied in the past years [2,6,7,10,16,17]. The general crystal structures of pyroxenes consist of the isolated chains of FeO_6 edge-sharing octahedra which lie parallel to the crystallographic $\boldsymbol{c}$ axis. The corner-sharing GeO_4 tetrahedra form infinite chains extended along the crystallographic $\boldsymbol{c}$ axis. These two types of chains alternate along the crystallographic $\boldsymbol{b}$ axis.

The room temperature crystal structure of $NaFeGe_2O_6$ is monoclinic with the space group $C2/c$ [17]. The crystal structure of the clinopyroxenes $LiFeGe_2O_6$ is monoclinic with the space group $P2_1/c$ at 300 K. $LiFeGe_2O_6$ undergoes a phase transition from $C2/c$ to $P2_1/c$ symmetry at $T=789$ K [10]. Noteworthy, the $C2/c$ and $P2_1/c$ structures differ in the configuration of the tetrahedral chains: in

* Corresponding author at: L.V. Kirensky Institute of Physics, SB RAS, Akademgorodok 50/38, Krasnoyarsk, 660036, Russia.
E-mail addresses: tvd@iph.krasn.ru (T.V. Drokina), msmolokeev@gmail.com (M.S. Molokeev).

http://dx.doi.org/10.1016/j.jmmm.2015.03.016
0304-8853/

$P2_1/c$ pyroxenes there are different, in $C2/c$ pyroxenes structure they are symmetric equivalent.

The magnetism of these chain pyroxenes is determined by the magnetic moment of the Fe^{3+} ions (S=5/2). $NaFeGe_2O_6$ clinopyroxenes orders below $T_N \approx 13$ K and the magnetic structure has been determined using neutron powder diffraction [6,16,7]. It is incommensurateand consists of antiferromagnetically coupled Fe^{3+} pairs with helical modulation within the [0,1] plane of the crystal lattice at 1.6 K > T > 11.5 K [16]. $LiFeGe_2O_6$ orders below $T_N \approx 20$ K [2]. The magnetic structure of $LiFeGe_2O_6$ is different to that observed for $NaFeGe_2O_6$. It does not exhibit an incommensurate modulation, but is a collinear antiferromagnetic structure with magnetic unit cell doubled along the ***a***-direction in the crystal [2].

Cation substitution influences structural and electronic properties of the pyroxenes and the study of intermediate phases often allows to identify the fundamental interactions driving the phase transitions and the influence of chemical pressure on the electronic properties. $Na_{0.5}Li_{0.5}FeGe_2O_6$ solid solution was first prepared by Novikov et al. [18] However, the detailed crystallographic structure and the magnetic ground state have been unknown so far.

In this paper, in order to characterize the properties of the solid solution $Na_{0.5}Li_{0.5}FeGe_2O_6$, we report the results from X-ray and neutron powder diffraction, as well as magnetization and calorimetric measurements. The relevant structural phase transition from $C2/c$ to $P2_1/c$ symmetry, the low temperature $P2_1/c$ crystal structure (G_1 phase), the crystallographic details of the crystal structure $C2/c$ (G_0 phase), magnetic properties and magnetic structure with the space group P_a2_1/c (G_2 phase) of the $Na_{0.5}Li_{0.5}FeGe_2O_6$ are reported herein.

2. Experimental

2.1. Material synthesis

The samples of $Na_{0.5}Li_{0.5}FeGe_2O_6$ were prepared by the solid-phase reaction method from a stoichiometric mixture of oxides Fe_2O_3, Na_2CO_3, $Li_2CO_3$and GeO_2. The powder was pressed into pellets which were subject to a high-temperature treatment at a maximum temperature of 1000 °C in air with several intermediate grindings. The chemical and phase composition of the pellet milled into the powder was examined by X-ray diffraction and shows a single phase.

2.2. X-ray diffraction

The X-ray powder diffraction data of $Na_{0.5}Li_{0.5}FeGe_2O_6$ for Rietveld analysis were collected between 133 K and 373 K with a Bruker D8 ADVANCE powder diffractometer (Cu-Kα radiation) and linear VANTEC detector. The step size of 2θ was 0.016°, and the total counting time of the scan was 3.6 h, with a 2θ range of $5° \le 2\theta \le 120°$. Additional 10 temperature steps for cell parameter evaluation were measured in the range from 133 K to 373 K with the total counting time 1.2 h. All refinements of the powder patterns were performed with TOPAS 4.2 (Bruker) [19].

2.3. Neutron diffraction

The neutron scattering experiments in the temperature range of 1.6–300 K, with a 2θ range of $5° \le 2\theta \le 92.7°$, and step width 0.1° were performed on the cold neutron powder diffractometer DMC [20] at the Swiss spallation neutron source SINQ [21]. The $Na_{0.5}Li_{0.5}FeGe_2O_6$ powder sample was enclosed in a cylindrical vanadium container under helium atmosphere and mounted in a helium cryostat. The neutron wavelength used was λ=2.44955 Å. The data has been corrected for absorption and was refined using the FULLPROF program package with the main aim to determine the magnetic phase at low temperature [22].

2.4. Magnetic bulk measurements

The magnetic properties measurements were performed on an SQUID magnetometer in the temperature range 4.0–300 K in magnetic field of 500 Oe.

2.5. Calorimetric measurements

The temperature dependence of the heat capacity $\Delta C_p(T)$ of $Na_{0.5}Li_{0.5}FeGe_2O_6$ was measured using differential scanning microcalorimeter DSM-10 Ma (DSM) in the temperature range from 100 K to 400 K. The experiments were performed in a helium atmosphere on a powder sample with a weight of 47 mg in the dynamic mode with heating and cooling rates of 16 K/min. The sample was packed in an aluminum container without any heat conducting greases.

To obtain the integral thermodynamic characteristics associated with phase transition, initially, the heat flow through the sample and reference compound was recorded against temperature. Then, after elimination of background, the information on excess heat capacity ΔC_p was obtained by processing the calorimetric results. The average deviation of the experimental data from the smoothed curve $\Delta C_p(T)$ does not exceed 1%. The error in the determination of the integral characteristics (enthalpy and entropy) is around ~10%.

3. Results and discussion

3.1. G_0 phase characterization

The X-ray powder pattern of $Na_{0.5}Li_{0.5}FeGe_2O_6$ at 300 K (G_0 phase) reveals that $Na_{0.5}Li_{0.5}FeGe_2O_6$ has the centrosymmetric $C2/c$ space group with 4 formula units per the cell and the lattice parameters are close to those of $NaFeGe_2O_6$ [7,17]. Therefore the crystal structure of $NaFeGe_2O_6$ was used as the starting model for the Rietveld refinement of the room temperature crystal structure of $Na_{0.5}Li_{0.5}FeGe_2O_6$. The site of Na-ion was occupied by Li- and Na-ions with fixed occupation p_{Li}=0.5 and p_{Na}=0.5, respectively. Anisotropic model of the preferred orientation effect with spherical harmonics 4 order was used [19]. The refinement was stable and gave low R-factors (Table 1, Fig. 1). Coordinates of atoms and main bond lengths are given in Tables 2 and 3 respectively. Additional Rietveld refinement of the G_0 phase using neutron data also showed good agreement between data and model (Fig. 2).

3.2. G_1 phase characterization

Analysis of X-ray patterns of $Na_{0.5}Li_{0.5}FeGe_2O_6$ measured from 133 K to 373 K showed the appearance of superstructure peaks at T_1=271.5 K which are forbidden in the G_0 phase with $C2/c$ space group (Fig. 3). This clearly indicates that the studied pyroxene undergoes a structural phase transition. The X-ray powder pattern at 133 K with increased statistics was used to obtain cell parameters and space group of the distorted phase G_1. In this phase $Na_{0.5}Li_{0.5}FeGe_2O_6$ has the centrosymmetric $P2_1/c$ space group with 4 formula units per cell and the cell parameters are close to those of $LiFeGe_2O_6$ [11] in G_1 phase, so this crystal structure was used as the starting model for Rietveld refinement. Anisotropic model of the preferred orientation effect with spherical harmonics 4 order was used. Small impurity of ice was detected on the pattern, and these peaks were accounted during refinement by using second

Table 1
Main parameters of processing and refinement of the $Na_{0.5}Li_{0.5}FeGe_2O_6$ sample.

Phase	G_0	G_1	G_2
Source	X-ray	X-ray	Neutron
Wavelength (Å)	1.5406	1.5406	2.44955
T (K)	300	133	1.5
Sp.Gr.	*C2/c*	$P2_1/c$	P_a2_1/c (14.80)
a (Å)	10.0333(1)	9.9692(3)	19.8314(8)
b, (Å)	8.8136(1)	8.8545(3)	8.8161(4)
c, (Å)	5.52965(9)	5.4752(2)	5.4471(3)
β, °	108.921(1)	108.494(1)	109.509(5)
V, (Å)^3	462.56(1)	458.34(3)	903.09(7)
Z	4	4	8
2θ-interval, (°)	5–120	5–120	5–92.7
No. of reflections	349	680	147
No. refinement parameters	53	96	50
R_{wp}, (%)	3.59	3.92	8.54
R_p, (%)	2.67	2.84	7.77
R_{exp}, (%)	2.14	2.34	1.34
χ^2	1.68	1.68	6.37
R_B, (%)	1.85	1.53	2.49
$R_{B\ magnetic}$, (%)	–	–	6.21

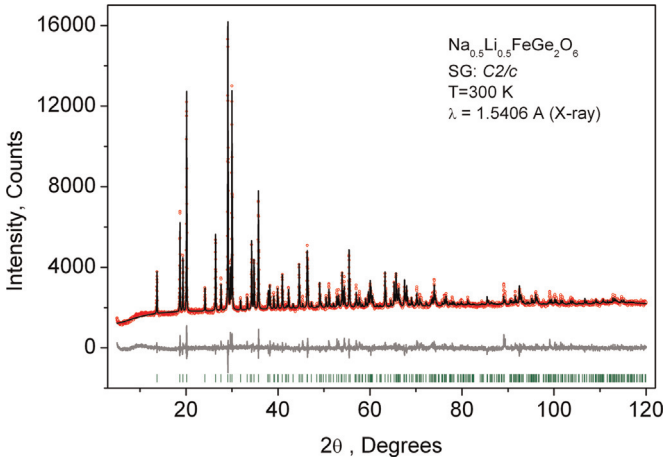

Fig. 1. Difference X-ray Rietveld plot of $Na_{0.5}Li_{0.5}FeGe_2O_6$ in G_0 phase (*C2/c*).

Table 2
Atomic coordinates and isotropic displacement parameters (Å^2) of $Na_{0.5}Li_{0.5}FeGe_2O_6$.

	x	*y*	*z*	B_{iso}	Occ.
T=300 K, *C2/c*					
Li	0	0.292 (2)	0.25	0.5 (4)	0.5
Na	0	0.292 (2)	0.25	0.5 (4)	0.5
Fe	0	0.9063 (5)	0.25	0.5 (2)	1
Ge	0.2878 (2)	0.0920 (3)	0.2381 (5)	0.5 (2)	1
O1	0.1009 (8)	0.091 (1)	0.163 (2)	1.0 (3)	1
O2	0.360 (1)	0.274 (1)	0.308 (2)	1.0 (3)	1
O3	0.343 (1)	0.003 (1)	0.033 (4)	1.0 (3)	1
T=133 K, $P2_1/c$					
Li	0.228 (3)	0.033 (2)	0.192 (6)	0.5 (5)	0.5
Na	0.228 (3)	0.033 (2)	0.192 (6)	0.5 (5)	0.5
Fe	0.260 (1)	0.6546 (6)	0.222 (2)	0.5 (2)	1
Ge1	0.0435 (8)	0.341 (1)	0.253 (2)	0.5 (2)	1
Ge2	0.5447 (7)	0.846 (1)	0.237 (3)	0.5 (2)	1
O1	0.876 (3)	0.349 (3)	0.204 (6)	1.5 (3)	1
O2	0.118 (3)	0.526 (4)	0.318 (7)	1.5 (3)	1
O3	0.085 (3)	0.241 (3)	0.546 (7)	1.5 (3)	1
O4	0.364 (3)	0.807 (3)	0.135 (7)	1.5 (3)	1
O5	0.603 (3)	1.015 (4)	0.334 (8)	1.5 (3)	1
O6	0.620 (3)	0.713 (3)	0.515 (6)	1.5 (3)	1

Table 3
Main bond lengths (Å) of $Na_{0.5}Li_{0.5}FeGe_2O_6$.

T=300 K, G_0 phase *C2/c*			
Li–O1	2.17 (2)	Fe–O2^{ii}	1.935 (9)
Li–O2^{i}	2.46 (1)	Ge–O1	1.784 (5)
Li–O3^{ii}	2.48 (2)	Ge–O2	1.75 (1)
Fe–O1^{iii}	2.06 (1)	Ge–O3	1.62 (1)
Fe–O1^{iv}	2.18 (1)	Ge–O3^{v}	1.75 (2)
T=133 K, G_1 phase $P2_1/c$			
Fe–O1^{i}	2.29 (3)	Li–O6^{vii}	2.90 (4)
Fe–O1^{ii}	2.30 (3)	Li–O6^{iv}	2.68 (3)
Fe–O2	2.01 (3)	Ge1–O1^{viii}	1.61 (2)
Fe–O4	1.85 (2)	Ge1–O2	1.79 (3)
Fe–O4^{iii}	2.20 (4)	Ge1–O3	1.76 (4)
Fe–O5^{iv}	1.94 (3)	Ge1–O3^{v}	1.51 (3)
Li–O1^{iv}	2.11 (3)	Ge2–O4	1.74 (2)
Li–O2^{v}	2.06 (5)	Ge2–O5	1.63 (3)
Li–O3^{v}	2.44 (3)	Ge2–O6	1.88 (3)
Li–O4^{vi}	2.49 (3)	Ge2–O6^{ix}	1.70 (3)
Li–O5^{vii}	2.64 (5)		

Symmetry codes: (1) G_0 phase (i) $-x+1/2$, $-y+1/2$, $-z+1$; (ii) $-x+1/2$, $y+1/2$, $-z+1/2$; (iii) x, $y+1$, z; (iv) $-x$, $-y+1$, $-z$; (v) x, $-y$, $z+1/2$; (2) G_1phase (i) $-x+1$, $-y+1$, $-z$; (ii) $-x+1$, $y+1/2$, $-z+1/2$; (iii) x, $-y+3/2$, $z+1/2$; (iv) $-x+1$, $y-1/2$, $-z+1/2$; (v) x, $-y+1/2$, $z-1/2$; (vi) x, $y-1$, z; (vii) $-x+1$, $-y+1$, $-z+1$; (viii) $x-1$, y, z; (ix) x, $-y+3/2$, $z-1/2$.

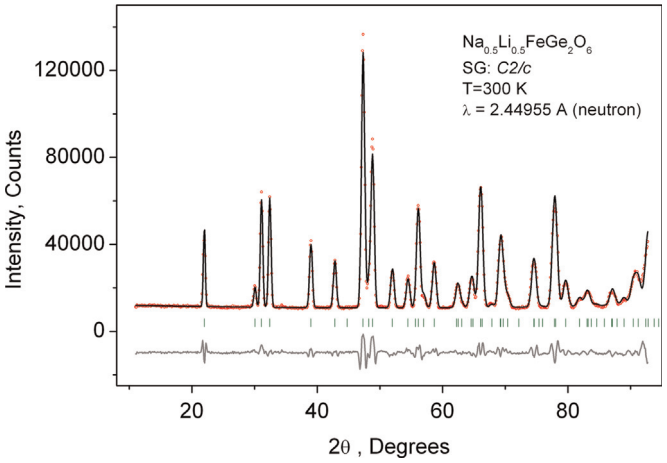

Fig. 2. Difference neutron Rietveld plot of $Na_{0.5}Li_{0.5}FeGe_2O_6$ in G_0 phase (*C2/c*) measured on DMC at SINQ.

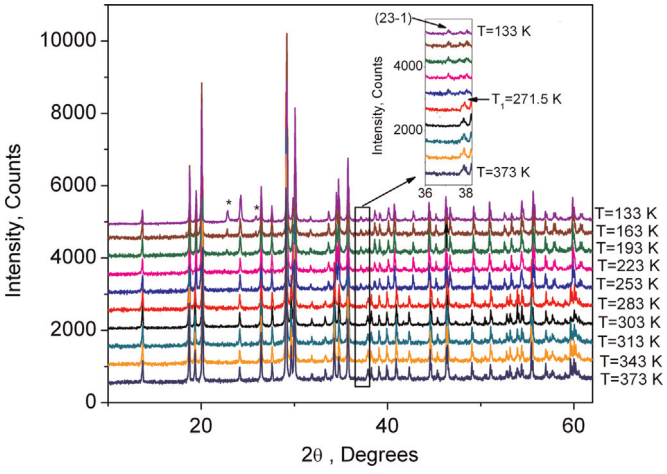

Fig. 3. X-ray patterns of $Na_{0.5}Li_{0.5}FeGe_2O_6$ measured from 133 K to 373 K, impurity peaks of ice are marked by stars. Inset shows the appearance of the superstructure peak at T_1=271.5 K which is forbidden in the G_0 phase (*C2/c*) but not forbidden in the G_1 phase ($P2_1/c$).

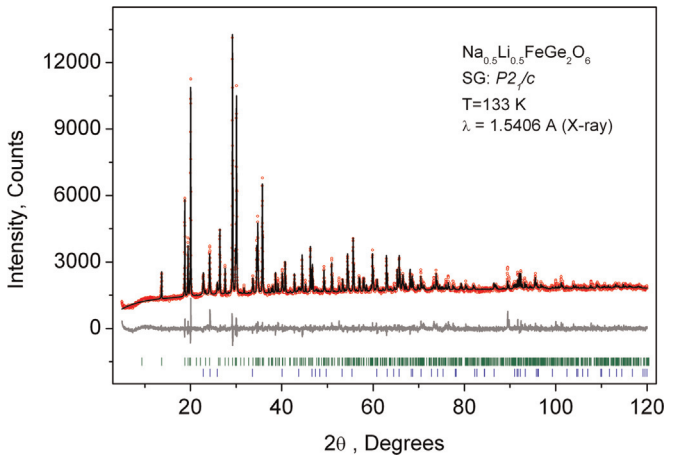

Fig. 4. Difference X-ray Rietveld plot of $Na_{0.5}Li_{0.5}FeGe_2O_6$ in G_1 phase (green sticks) with small impurity of ice (blue sticks below). (For interpretation of the references to color in this figure legend, the reader is referred to the web version of this article.)

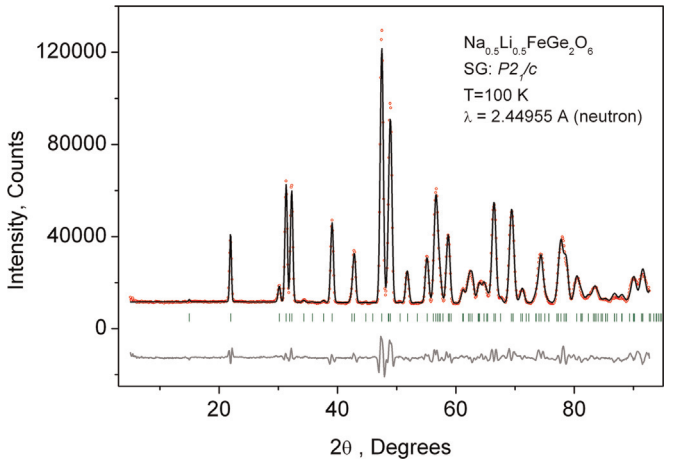

Fig. 5. Difference neutron Rietveld plot of $Na_{0.5}Li_{0.5}FeGe_2O_6$ in G_1 phase ($P2_1/c$) measured on DMC at SINQ.

phase. Refinement was stable and gave low R-factors (Table 1, Fig. 4). The coordinates of atoms and main bond lengths are given in Tables 2 and 3 respectively. The Rietveld refinement of the G_1 phase using neutron data also showed good agreement and confirms the suggested model of the structure (Fig. 5). The temperature dependence of the cell parameters (Fig. 6) and the cell volume (Fig .7) show a jump at the phase transition which proves the first order character of the phase transition $G_0 \rightarrow G_1$.

In order to further characterize the phase transformation between the pyroxene structures we have investigated the thermal properties of the $Na_{0.5}Li_{0.5}FeGe_2O_6$ compound. The results of calorimetric investigations in the temperature range from 100 K to 400 K revealed one anomaly in the heat capacity, which is connected with the phase transition, and is presented in Fig. 8a. The temperature dependence of the excess heat capacity was calculated after extraction of the lattice heat capacity C_{lat} which was approximated by a smooth polynomial function. A good agreement was found between calculated C_{lat} and experimental data away from the phase transition. In heating mode, the anomaly of the heat capacity ΔC_p was observed at $T=276\pm1$ K (red line in Fig. 8a). Measurements carried out in cooling mode revealed an anomaly at $T=271\pm1$ K (blue line in Fig. 8a). So the corresponding temperature hysteresis is about 5 K and proves the first-order character of the phase transition.

The excess enthalpy is characterized by the following value: $\Delta H=\int \Delta C_p(T)dT=(530\pm50)$ J/mol. The entropy ΔS corresponding to the anomalous behavior of the heat capacity was calculated by integrating the function $(\Delta C_p/T)(T)$ and is shown in Fig. 8b. The small value of the phase transition entropy $\Delta S=1.9$ J/molK $\approx 0.2R$ (R is molar gas constant) indicates the displacive nature of the crystal transformation [23].

The characteristics of the $C2/c \rightarrow P2_1/c$ phase transition has been previously investigated in the isostructural compound $LiFeSi_2O_6$ [24], however the critical mode which is responsible for the phase transition was neither found nor described. Therefore, this analysis is performed herewith the data from $Na_{0.5}Li_{0.5}FeGe_2O_6$, but believed to be similar for all $C2/c \rightarrow P2_1/c$ transitions in pyroxenes. Mode decomposition of the distorted G_1 phase ($P2_1/c$) in terms of the undistorted parent structure G_0 ($C2/c$) was performed using the ISODISTORT program [25]. It was found that the basis set of distorted and parent phases doesn't change: $\boldsymbol{a_1}=\boldsymbol{a_0}$; $\boldsymbol{b_1}=\boldsymbol{b_0}$, $\boldsymbol{c_1}=\boldsymbol{c_0}$, where ($\boldsymbol{a_1}$, $\boldsymbol{b_1}$, $\boldsymbol{c_1}$) and ($\boldsymbol{a_0}$, $\boldsymbol{b_0}$, $\boldsymbol{c_0}$) are basis of distorted and parent phases respectively, however the origin shifts (1/4; 1/4; 0) (Fig. 5a, b). Only two modes were found: $\Gamma_1^+(\varepsilon)$ and $Y_2^-(\eta)$ with their overall displacive mode amplitudes are 0.94 and 1.48, respectively. Here, Γ and Y are points in the Brillouin zone of the parent phase $C2/c$ with the coordinates (0, 0, 0) and (0, 1, 0), respectively. The ε and η are order parameters. The mode with the largest displacement is the primary order parameter: $C2/c \overset{Y_2^-(\eta)}{\Longrightarrow} P2_1/c$. It gives rise to a splitting of the Wyckoff position occupied by the Ge atom into two sites, Ge1 and Ge2 (Fig. 9a, b). The largest displacements of the atoms are linked with $Ge1O_4$ and $Ge2O_4$ tetrahedra rotations which are driven by $Y_2^-(\eta)$ mode. There is no charge ordering of Li/Na and Fe ions accompanying this phase transition, only small shifts were detected.

So, G_0 ($C2/c$) $\rightarrow G_1$ ($P2_1/c$) first-order phase transition can be described as being displacive in character.

3.3. G_2 magnetic phase characterization

The magnetic properties indicate a magnetic transition from paramagnetic to magnetic ordered state in $Na_{0.5}Li_{0.5}FeGe_2O_6$ compound. The temperature dependence of magnetic moment M at the external field $H=500$ Oe is shown in Fig. 10a. The M (T) dependence of $Na_{0.5}Li_{0.5}FeGe_2O_6$ sample shows a broad maximum near $T=27.5$ K, which is the characteristic property of quasi-low-dimensional magnetic spin system, and an inflection point at $T=T_N=18$ K.

The measured temperature dependence of inverse magnetic susceptibility $\chi^{-1}(T)$ for $Na_{0.5}Li_{0.5}FeGe_2O_6$ is not linear at high temperatures, instead a sluggish deviation from linearity takes place in high temperature range (above 200 K). This dependence can be described with adding of a temperature-independent constant in the Curie-Weiss law. The value of a temperature-independent constant was determined experimentally from $\chi(1/T)$ dependence (at $T\rightarrow\infty$ $\chi\rightarrow A$). It is assumed that A originates from the susceptibility of a small ferromagnetic impurity which is not detected by X-ray powder diffraction method similar to the contribution in susceptibility of pure $LiFeGe_2O_6$ [2]. After the correction the temperature dependence of the inverse magnetic susceptibility shows Curie-Weiss behavior at temperatures above 150 K (Fig. 10b). Fitting a linear regression line to the data, the asymptotic Néel temperature θ was found to be negative with $\theta=-14$ K which indicates the prevailing presence of the antiferromagnetic exchange interaction within the magnetic ions chains. The values of the effective magnetic moment, theoretical (μ_{cal}) and determined from experimental data (μ_{exp}), and other key magnetic data are given in Table 4.

Neutron powder diffraction below T_N finds a large number of additional Bragg peaks due to long-range order of the magnetic

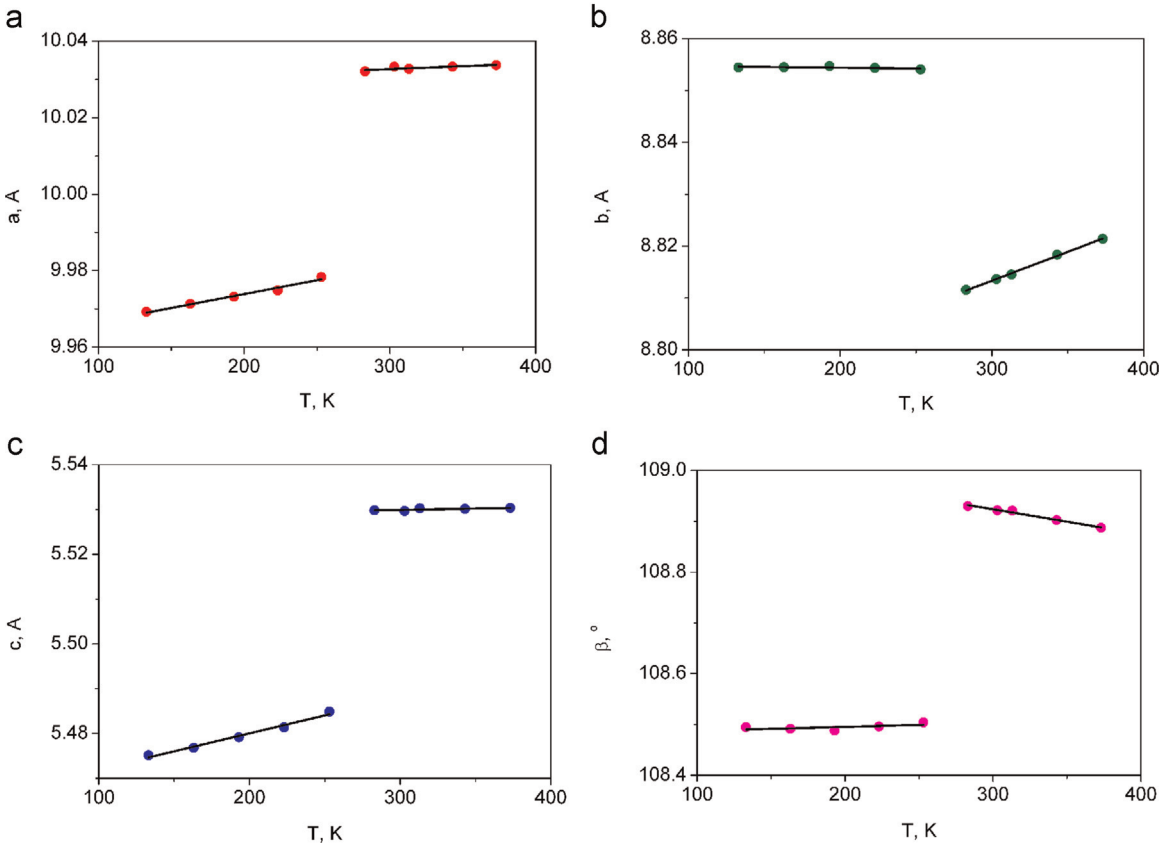

Fig. 6. Unit-cell parameters of $Na_{0.5}Li_{0.5}FeGe_2O_6$ as a function of temperature (a) a-cell parameter; ((b) b-cell parameter; (c) c-cell parameter; (d) monoclinic angle β) all characterizing the first-order phase transition from $P2_1/c$ to $C2/c$.

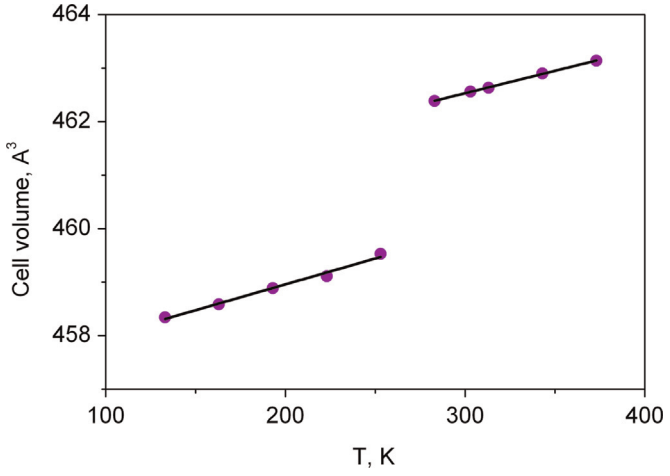

Fig. 7. Temperature dependence of cell volume in $Na_{0.5}Li_{0.5}FeGe_2O_6$.

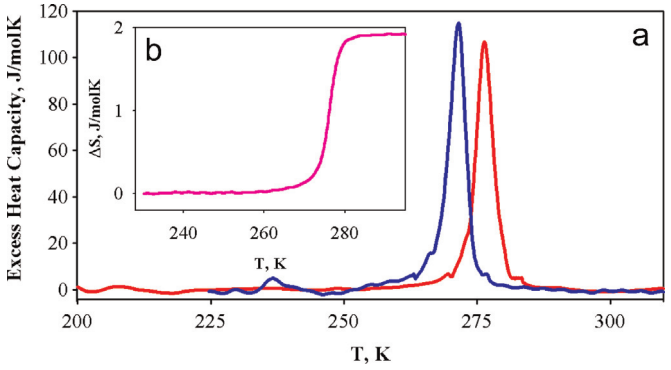

Fig. 8. Temperature dependences of the excess heat capacity ΔC_p and the excess entropy ΔS (inset) of $Na_{0.5}Li_{0.5}FeGe_2O_6$ measured in the heating mode (red line) and in the cooling mode (blue line). (For interpretation of the references to color in this figure legend, the reader is referred to the web version of this article.)

moments in the $Na_{0.5}Li_{0.5}FeGe_2O_6$ clinopyroxene (Fig. 11). The temperature dependence of the strongest magnetic peak is shown in Fig. 12, revealing the onset of the magnetic order near 18 K. This is in accordance with the results of SQUID magnetic measurements of $Na_{0.5}Li_{0.5}FeGe_2O_6$ (Fig. 10).

The magnetic reflections positions can be indexed by doubling the unit cell along the *a*-axis, i.e. a propagation vector $\boldsymbol{k}=(1/2, 0, 0)$: $\boldsymbol{a_2}=2\times\boldsymbol{a_0}$; $\boldsymbol{b_2}=\boldsymbol{b_0}$, $\boldsymbol{c_2}=\boldsymbol{c_0}$, where ($\boldsymbol{a_2}$, $\boldsymbol{b_2}$, $\boldsymbol{c_2}$) and ($\boldsymbol{a_0}$, $\boldsymbol{b_0}$, $\boldsymbol{c_0}$) are basis of the distorted magnetic and the parent phases, respectively. The possible magnetic space groups were generated by using ISODISTORT program [24], and only P_a2_1/c satisfies all conditions. There are two settings or notations currently in use for magnetic space groups: (1) the OG setting refers to the Opechowski-Guccione notation (symmetry operations referred to a unit cell which the crystal would have if the magnetic order is neglected); (2) the BNS setting refers to the Belov-Neronova-Smirnova notation (the magnetic unit cell is in general different from the crystallographic one). The P_a2_1/c space group belongs to the BNS notation and can be transformed to $P2'_1/c$ in OG notation. The $P2'_1/c$ space group was previously used to solve the magnetic crystal structure of $LiFeGe_2O_6$ [2]. Since the neutron data in (Ref. [2]) are close to our pattern, the magnetic structures are the same. However, here the magnetic structure is solved and refined in the BNS notation which is more convenient for presentation, comparison and analyzing. So, the initial magnetic structure of the G_2 (P_a2_1/c) phase was generated by using ISODISTORT and utilized as input to find the real magnetic structure by simulated annealing in

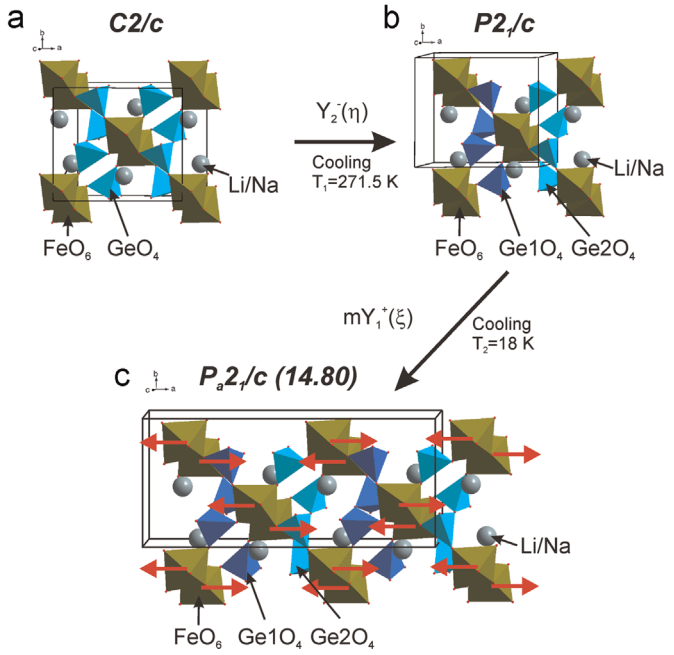

Fig. 9. Crystal structures of (a) G_0 phase ($C2/c$); (b) G_1 phase ($P2_1/c$); (c) G_2 phase (P_a2_1/c) where red arrows show the magnetic moment of Fe ions. Big black arrows show phase transitions under cooling. Critical modes which distort the crystal structure at phase transitions are indicated near the arrows.

Fullprof [22]. The final model of both the crystallographic and magnetic structure was refined by Rietveld method in Fullprof program. The refinement was stable and gave low R-factors (Table 1, Fig. 13). Coordinates of atoms and obtained magnetic momentum are listed in Table 5.

As mentioned before, the comparison of the magnetic crystal structures of $Na_{0.5}Li_{0.5}FeGe_2O_6$ (Fig. 9) and $LiFeGe_2O_6$ [7] showed that they are the same. However, BNS notation allows the mode decomposition of the distorted G_2 phase using the ISODISTORT program. There are eight magnetic modes which can distort the crystal structure: $m\Gamma_1^+$; $m\Gamma_2^+$; $m\Gamma_1^-$; $m\Gamma_2^-$; mY_1^+; mY_2^+; mY_1^-; mY_2^-, but only one $mY_1^+(\xi)$ has a non-zero amplitude after decomposition of the magnetic structure by ISODISTORT. This mode is critical at the magnetic phase transition. Therefore, $mY_1^+(\xi)$ mode leads to the antiferromagnetic ordering observed in both the $Na_{0.5}Li_{0.5}FeGe_2O_6$ and $LiFeGe_2O_6$ compounds.

In summary, the whole sequence of the phase transitions observed in $Na_{0.5}Li_{0.5}FeGe_2O_6$ can be presented in the form:

Table 4
Magnetic characteristics of $Na_{0.5}Li_{0.5}FeGe_2O_6$.

θ, K	T_N, K	T_{max}, K	$\mu_{exp.}$, μ_B	$\mu_{calc.}$, μ_B
−14	18	27.5	4.5	5.9

Note: θ is the asymptotic Néel temperature, T_N is the Néel temperature, T_{max} is temperature corresponding to the maximum magnetic moment value, μ_{exp} is the experimental effective magnetic moment, μ_{calc} is the calculated effective magnetic moment

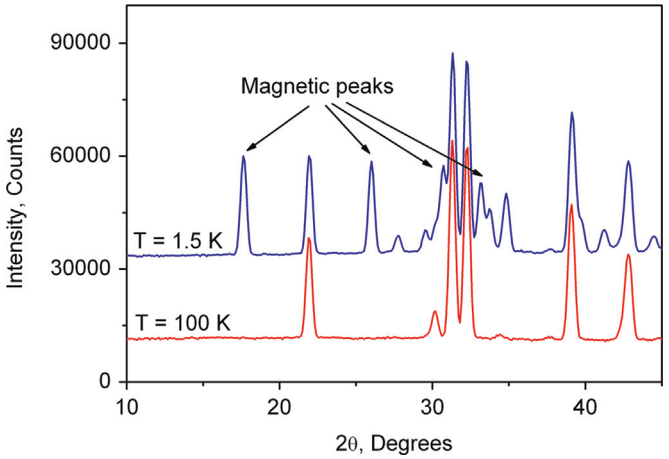

Fig. 11. Fragment of neutron diffraction patterns, showing the appearance of the magnetic scattering of $Na_{0.5}Li_{0.5}FeGe_2O_6$ in G_2 phase.

$$C2/c \overset{Y_2^-(\eta)}{\Longrightarrow} P2_1/c \overset{mY_1^+(\xi)}{\Longrightarrow} P_a2_1/c$$ (Fig. 9).

4. Conclusions

Two phase transitions were observed and characterized in the clinopyroxene $Na_{0.5}Li_{0.5}FeGe_2O_6$ through X-ray and neutron powder diffraction, calorimetric and magnetic methods.

The first phase transition is structural phase transition changing the symmetry from $C2/c$ to $P2_1/c$ at $T=271$ K. The temperature dependences of the cell parameters and the volume, the appearance of $h+k$ odd reflections with decreasing temperature, forbidden in $C2/c$ symmetry but allowed in $P2_1/c$ symmetry, as well as the thermal properties indicated that the $C2/c$ to $P2_1/c$ transformation occurs and is first order and displacive type in character. The most significant difference between the G_0 to G_1 phase structures is, beneath the crystal symmetry, the kinking of

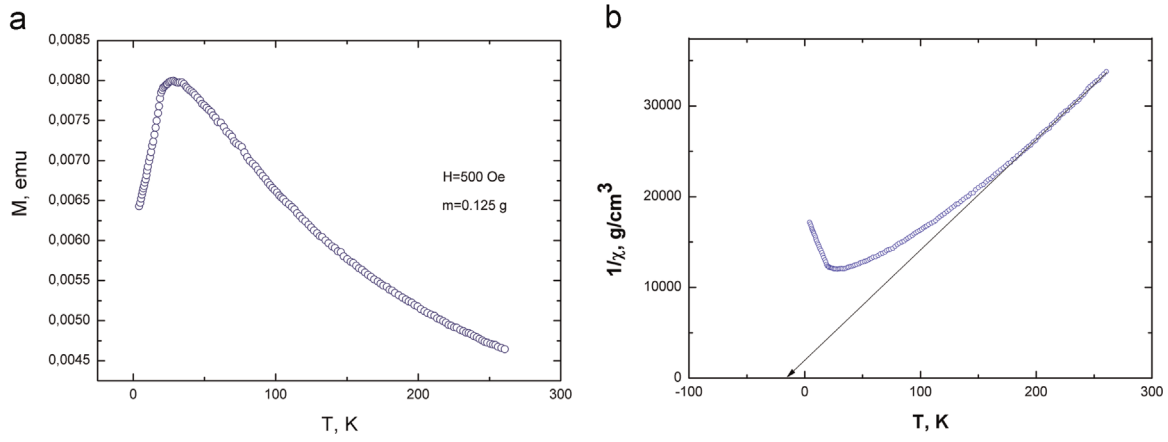

Fig. 10. The temperature dependencies of magnetic moment (a) and inverse magnetic susceptibility (b) of $Na_{0.5}Li_{0.5}FeGe_2O_6$ in the magnetic field $H=500$ Oe after corrections have been applide (see text). The ordering temperature is $T_N=18$ K. The sample mass is $m=0.125$ g.

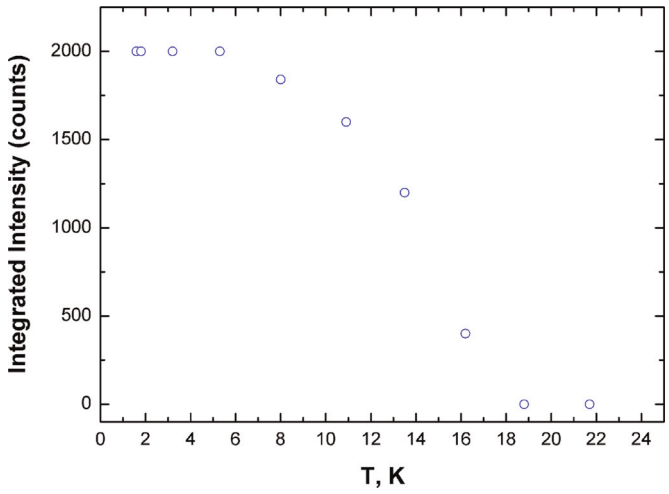

Fig. 12. Intensity of the strongest magnetic peak $(1, 1, 0) \pm \mathbf{k}$ of $Na_{0.5}Li_{0.5}FeGe_2O_6$ determined by neutron diffraction as a function of temperature, Néel temperature $T_N \approx 18$ K.

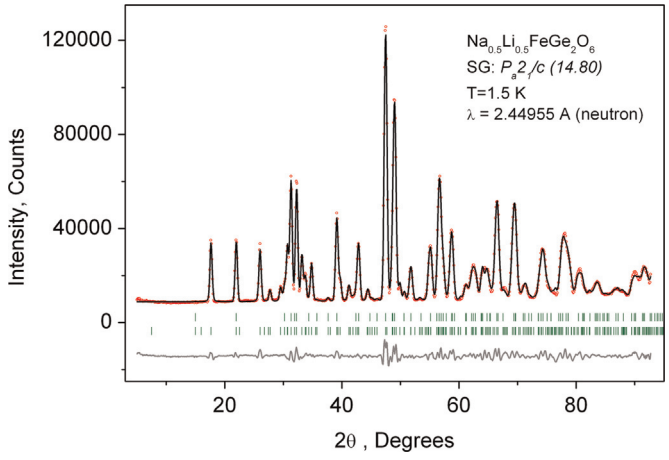

Fig. 13. Difference neutron Rietveld plot of $Na_{0.5}Li_{0.5}FeGe_2O_6$ in G_2 phase (P_a2_1/c) measured on DMC at SINQ.

Table 5
Fractional atomic coordinates, isotropic displacement parameters (Å^2) and magnetic moment per Fe^{3+} ion of $Na_{0.5}Li_{0.5}FeGe_2O_6$ at $T = 1.5$ K.

	x	y	z	B_{iso}	Occ.	M_x, μ_B	M_y, μ_B	M_z, μ_B
Li	0.13 (2)	0.064 (6)	0.26 (2)	0.5	0.5	–	–	–
Na	0.13 (2)	0.064 (6)	0.26 (2)	0.5	0.5	–	–	–
Fe	0.12 (2)	0.6525 (5)	0.230 (1)	0.5	1	4.30(4)	0	0
Ge1	0.020 (2)	0.340 (2)	0.249 (3)	0.5	1	–	–	–
Ge2	0.274 (2)	0.844 (2)	0.241 (2)	0.5	1	–	–	–
O1	0.427 (2)	0.329 (3)	0.158 (3)	0.5	1	–	–	–
O2	0.052 (2)	0.519 (2)	0.285 (2)	0.5	1	–	–	–
O3	0.055 (1)	0.279 (1)	0.573 (2)	0.5	1	–	–	–
O4	0.182 (2)	0.836 (3)	0.116 (3)	0.5	1	–	–	–
O5	0.311 (2)	0.020 (2)	0.340 (2)	0.5	1	–	–	–
O6	0.309 (1)	0.710 (1)	0.494 (2)	0.5	1	–	–	–

$Ge1O_4$ and $Ge2O_4$ chains and a passive role of the Na, Li, Fe cations. The structural transition is driven by the $Y_2^-(\eta)$ mode in the $Na_{0.5}Li_{0.5}FeGe_2O_6$ compound. For both crystallographic structures the main parameters were obtained.

The second phase transition is the transition from the paramagnetic state to the antiferromagnetic long-range ordered state occurring at $T_N = 18$ K. The $Na_{0.5}Li_{0.5}FeGe_2O_6$ magnetic structure has been determined at $T = 1.5$ K, but there is indication for a change in the magnetic structure with temperature. $Na_{0.5}Li_{0.5}FeGe_2O_6$ orders in a collinear antiferromagnetic structure, with a magnetic space group P_a2_1/c and the propagation vector $\mathbf{k} = (1/2, 0, 0)$. The critical mode which leads to antiferromagnetic ordering has been found ($mY_1^+(\xi)$ mode). Since the magnetic order of $LiFeGe_2O_6$ seems identical, the ordering there is also linked to the critical mode $mY_1^+(\xi)$. The observed magnetic structure is 3-dimensional, however, the reduced ordered magnetic moment indicates remaining disorder in the low-dimensional magnet $Na_{0.5}Li_{0.5}FeGe_2O_6$.

The studies of this chain clinopyroxene solid solution allow to better understand the relationship of structure and magnetic properties. The lower chemical pressure of the Li-doped compound destabilizes the $C2/c$ structure and leads to the structural phase transition, while apparently the magnetic structure is a consequence of the lower symmetry of the $P2_1/c$ crystal structure. It would be interesting to investigate a $Na_{1-x}Li_xFeGe_2O_6$ compound where structural and magnetic phase transitions occur in the same temperature range.

Acknowledgements

Neutron beam time at the cold neutron powder diffractometer DMC at the Swiss spallation neutron source SINQ, Paul Scherrer Institut, Switzerland is gratefully acknowledged. MF acknowledges funding from the European Community's Seventh Framework Programme (FP7/2007-2013) under Grant Agreement no. 290605 (PSIFELLOW/COFUND).This work was also supported by Ministry of Education and Science of the Russian Federation of Siberian Federal University 2014 year (Assignment no. 3.2534.2014/K).

References

[1] E. Baum, W. Treutmann, M. Behruzi, W. Lottermoser, G. Amthauer, FurKristal 183 (1988) 273.
[2] G.J. Redhammer, G. Roth, W. Treutmann, M. Hoelzel, W. Paulus, G. Andre, C. Pietzonka, G. Amthauer, J. Solid State Chem. 182 (2009) 2374.
[3] A.N. Vasiliev, O.L. Ignatchik, A.N. Sokolov, Z. Hiroi, M. Isobe, Y. Ueda, Phys. Rev. B 72 (2005) 012412.
[4] A.N. Vasiliev, O.L. Ignatchik, M. Isobe, Y. Ueda, Phys. Rev. B 70 (2004) 132415.
[5] G. Nenert, C. Ritter, M. Isobe, O. Isnard, A.N. Vasiliev, Y. Ueda, Phys. Rev. B 80 (2009) 024402.
[6] T. Drokina, G. Petrakovskii, L. Keller, J. Schefer, J. Phys.: Conference Ser. 251 (2010) 012016.
[7] G.J. Redhammer, A. Senyshyn, M. Meven, G. Roth, S. Prinz, A. Pachler, G. Tippelt, C. Pietzonka, W. Treutmann, M. Hoelzel, B. Pedersen, G. Amthauer, Phys. Chem. Miner. 38 (2011) 139.
[8] M. Isobe, E. Ninomiya, A.N. Vasiliev, Y. Ueda, J. Phys. Soc. Japan 71 (2002) 1423.
[9] S.V. Streltsov, D.I. Khomskii, Phys. Rev. B 77 (2008) 064405.
[10] G.J. Redhammer, F. Cámara, M. Alvaro, F. Nestola, G. Tippelt, S. Prinz, J. Simons, G. Roth, G. Amthauer, Phys. Chem. Minerals 37 (2010) 685.
[11] F. Nestola, G.J. Redhammer, M.G. Pamato, L. Secco, A. dal Negro, American Mineralogist 94 (2009) 616.
[12] T. Arlt, R.J. Angel, Phys. Chem. Minerals 27 (2000) 719.
[13] F. Nestola, T.B. Ballaran, H. Ohashi, Phys. Chem. Minerals 35 (2008) 477.
[14] I. Kim, B.-G. Jeon, D. Patil, S. Patil, G. N´enert, K.H. Kim, J. Phys.: Condens. Matter 24 (2012) 306001.
[15] S. Jodlauk, P. Becker, J.A. Mydosh, D.I. Khomskii, T. Lorenz, S.V. Streltsov, D.C. Hezel, L. Bohaty, J. Phys. Cond. Matter. 19 (2007) 432.
[16] T.V. Drokina, G.A. Petrakovskii, L. Keller, J. Schefer, A.D. Balaev, A.V. Kartashev, D. A. Ivanov, JETP 112 (2011) 121.
[17] L. Solovyova, V. Bakakin, Krystallographiya (Rus) 12 (1967) 591.
[18] G.V. Novikov, L.V. Sipavina, Vestnik of Earth Science Department RAN 1 (21) (2003) 1.
[19] Bruker A.X.S. TOPAS V4: General profile and structure analysis software for powder diffraction data. – User's Manual. Bruker AXS, Karlsruhe, Germany (2008).
[20] P. Fischer, L. Keller, J. Scheffer, J. Kohlbrecher, Neutron News 11 (2000) 19.
[21] W.E. Fischer, Physica B 234-236 (1997) 1202.
[22] J. Rodriguez-Carvajal, J.Physica B: Condens. Matter. 192 (1993) 55.
[23] I.N. Flerov, M.V. Gorev, K.S. Aleksandrov, A. Tressaud, J. Grannec, M. Couzi, Materials Science and Engineering R24 (3) (1998) 81.
[24] G.J. Redhammer, G. Roth, W. Paulus, G. Andre, W. Lottermoser, G. Amthauer, W. Treutmann, B. Knoppelhuber-Bitschnau, Phys. Chem. Minerals 28 (2001) 337.
[25] B.J. Campbell, H.T. Stokes, D.E. Tanner, D.M. Hatch, J. Appl. Cryst. 39 (2006) 607.